Design and Characterization of Carbon Nanotube Based Ultra High Speed Nanomotor in Water

A thesis submitted to the

Department of Electrical and Electronic Engineering (EEE)

of

Bangladesh University of Engineering and Technology (BUET)

In partial fulfillment of the requirement for the degree of

MASTER OF SCIENCE IN ELECTRICAL AND ELECTRONIC ENGINEERING

by

Md. Mushfiqur Rahman

(Roll No.: 1015062232 P)

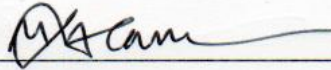DEPARTMENT OF ELECTRICAL AND ELECTRONIC ENGINEERING (EEE)

BANGLADESH UNIVERSITY OF ENGINEERING AND TECHNOLOGY (BUET)

November 2017

The thesis titled "**Design and Characterization of Carbon Nanotube Based Ultra High Speed Nanomotor in Water**" submitted by Md. Mushfiqur Rahman, Roll No.: 1015062232P, Session: October 2015, has been accepted as satisfactory in partial fulfillment of the requirement for the degree of MASTER OF SCIENCE IN ELECTRICAL AND ELECTRONIC ENGINEERING on November 01, 2017.
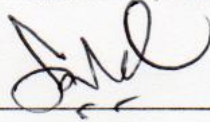
Board of Examiners

1. **Dr. Md. Kawsar Alam**   Chairman
                                                   (Supervisor)
   Associate Professor
   Department of Electrical & Electronic Engineering (EEE),
   BUET, Dhaka-1205, Bangladesh

2. **Dr. Quazi Deen Mohd Khosru**   Member
                                                   (Ex-officio)
   Professor and Head
   Department of Electrical & Electronic Engineering (EEE),
   BUET, Dhaka-1205, Bangladesh

3. **Dr. Samia Subrina**   Member

   Associate Professor
   Department of Electrical & Electronic Engineering (EEE),
   BUET, Dhaka-1205, Bangladesh

4. **Dr. Md. Sharafat Hossain**   Member
                                                   (External)
   Professor
   Department of Electrical & Electronic Engineering (EEE),
   DUET, Gazipur-1700, Bangladesh

Declaration

It is hereby declared that this thesis or any part of it has not been submitted elsewhere for the award of any degree or diploma.

Signature of the candidate

M Rahman

Md. Mushfiqur Rahman

(Roll No. 1015062232P)

Dedication

To my family

Acknowledgements

Abstract

This thesis proposes a carbon nanotube based novel nanomotor structure that is capable of rotating at an ultrahigh speed. Using molecular dynamics simulations, it is shown that a carbon nanotube (CNT) suspended in water and subjected to a rotating electric field of proper magnitude and angular speed, can be rotated with the aid of water dipole orientations. Based on this principle, we design a rotational nanomotor structure and simulate the system in water. We make use of the fast responsiveness of electric field induced CNT orientation in water and show its operation at ultrahigh-speed (over 10^{11} r.p.m.). To explain the basic mechanism, we also analyze the behavior of the rotational actuation originated from the water dipole orientation. The proposed nanomotor is capable of rotating an attached load (such as CNT) at a precise angle as well as nano-gear based complex structures. The findings suggest potential way of using the electric field induced CNT rotation in polarizable fluids as a novel tool to operate nano-devices and systems.

Preface

The following paper was published based on the contribution of this thesis.

- **M. M. Rahman**, M. M. Chowdhury, and M. K. Alam, "Rotating Electric Field Induced Carbon Nanotube Based Nanomotor in Water: A Molecular Dynamics Study", *Small,* **13**, pp. 226-241, 2017. (Publisher: Wiley, **Impact factor: 8.643**).

Necessary permission has been obtained from the respective publisher for incorporating the work/paper in this M.Sc. thesis.

TABLE OF CONTENTS

LIST OF FIGURES

LIST OF TABLES

Chapter 1

Introduction

In recent years, along with other electromechanical systems, the ubiquitous rotary device –

motor has also experienced the art of miniaturization, particularly the evolution from micro-

to nanoscale [1, 2]. This miniaturization, from microelectromechanical system (MEMS) to

nanoelectromechanical system (NEMS), has important implications because of its capability

of making scientific breakthroughs in various areas including nano-robotics, bio-NEMS and

nanofluidics [3-5]. In general, the MEMS are developed on the basis of traditional

photolithography and micromachining technologies which require hundreds of fabrication

steps and eventually result in low yield and short lifetime devices. As a result, it is difficult

to apply these fabrication technologies to the preparation of even smaller NEMS devices [1].

It is, therefore, important to investigate new principles and design approaches (e.g. device

preparation by using synthesized nanoentities as building blocks) to realize nanoscale

devices/systems like nanomotors [6]. However, among the reported schemes, the number of

nanomotor systems driven by electrical energy is very few and their performance is limited

by low lifetime, complex assembly process, lack of adequate propelling power to rotate

molecular scale loads etc. [6] An electrical energy driven nanomotor which is suitable to

operate in water and capable of exerting enough force to rotate the external load has not

been reported yet in literature. Such a nanomotor can be an exciting addition to the current

research on electrical energy driven NEMS devices, with its applications ranging from bio-

NEMS, microfluidics, nanofluidics architectures. to optical switching, memory devices, and nano-robotics [3-6].

1.1   Carbon Nanotubes (CNTs)

Carbon is the fundamental building block of life. A large number of complex molecules are made up of carbon bonded with other elements, such as oxygen, hydrogen, nitrogen etc. From the simple hydrocarbons to complex bio-molecules including proteins, lipids and DNA, carbon is omnipresent. In nature, carbon is found in different types of allotropes. If each atom covalently bonds to four other carbons, and forms a tetrahedral bond structure, the result is a diamond. Another well-known allotrope of carbon is Graphene. This allotrope has each atom covalently bonded to three other carbons in a hexagonal lattice forming one atom-thick planar structure. When these 2-D sheets are stacked on top of each other, the result is graphite [7]. Another stable form of carbon is Carbon Nanotubes (CNTs) [8]. CNTs can be thought of as a rolled up graphene sheet into a cylindrical tubular structure. Since their discovery in 1991, CNTs have attracted considerable interest, due to their exceptional mechanical, chemical, optical, and electronic properties that make them suitable for a wide range of applications including catalysis, electronics, and molecular sensing [8]. In general, CNTs are classified into two categories: Single-Walled Carbon Nanotubes (SWCNTs) and Multi-Walled Carbon Nanotubes (MWCNTs). While SWCNTs are made from a graphene sheet rolled into a cylinder, MWCNTs are composed of multiple concentric SWCNTs. SWCNTs are more expensive and difficult to manufacture when compared to MWCNTs. When carbon atoms geometrically combine together to form graphite, the sp^2 hybridization

of carbon atoms takes place. Different types of CNTs can be characterized by a linear combination of base vectors **a** and **b** of the hexagon, or **r**= n**a**+ m**b**, where n and m are integers of the vector equation [8-12]. The values of n and m uniquely determine the chirality, or twist style of the nanotube. Three major categories of CNTs can be defined based on the value of n and m. If $n = m$, the CNT is considered as armchair (Figure 1.1), if $n = 0$ or $m = 0$, the CNT is classified as zigzag. When $n \neq m$, the CNT is known as chiral. The chirality affects the conductance, density, lattice structure, and therefore affects other properties of the nanotube. Furthermore, a SWCNT is considered as metallic if the value (n-m) is divisible by three. Otherwise, the nanotube is semiconducting. The outstanding properties of CNTs make them very special in applications on a variety of fields. These properties along with the rigid structure make it ideal for an integrated chip design, biosensors, ion-transport channels, fuel storage, and for a varied range of other usages [13-15]. Besides, these nonpolar rigid structures can be used as unique molecular channels for water, ions, proteins, DNA, by changing the local channel polarity and solvent conditions [16-21]. Recently, CNT in water system has drawn a lot of interest because of its emerging applications in superfast water transport and water supply [16, 18].
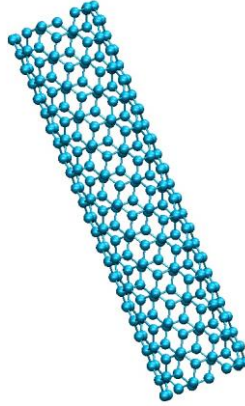
Figure 1.1. Snapshot of a (5,5) nanotube of length 3.0 nm.

1.2   Nano Electromechanical Systems (NEMS)

Nano-electromechanical systems (NEMS) are emerging new technologies promising for a number of scientific and technological applications [4]. NEMS can be regarded as the class of device having both electrical and mechanical functionalities with a size of several nanometers. The most common types of NEMS devices include nano- actuators, pumps, motors, oscillators, sensors, displays, transducers, energy harvesting devices etc. [1, 4, 22] These devices are created taking advantage of different physical principles such as optical, thermal, electrical, chemical etc. [22] In general, electromechanical systems are experiencing miniaturization in order to reduce mass, increase resonant frequency, and lower the force constants associated with these systems [22]. With the rapid advancement of modern science and technology, the traditional Micro Electromechanical Systems (MEMS) continued to shrink in size, leading to the development of NEMS technologies.

The earliest demonstration of a Very Large Scale Integration (VLSI) NEMS device was illustrated by IBM researchers back in 2000, where they developed an array of Atomic Force

Microscopy (AFM) tips [23]. Their device was able to sense a deformable substrate in order to function as a data storage device. Another extensively studied class of NEMS devices is nanoscale motors. Nanomotors can be particularly useful in various fields including nano-robotics, bio-NEMS and nanofluidics, targeted drug delivery, cargo-towing applications etc. [6, 22, 24-43] Another interesting class of NEMS is the sensing devices. While MEMS devices are large in size, it is fundamentally impossible to sense smaller nano sized entities. With the aid of modern NEMS sensors, smaller sized bio-molecules, even single celled organisms are able to be sensed with a reasonable level of precision [44]. Some of the common types of NEMS sensors are accelerometers, biochemical analyzers, gyroscopes, medical diagnostic sensors, pressure sensors etc. [45] NEMS can either be produced bottom-up (e.g. chemical self-assembly methods, CVD methods, hot plate technique), top-down (e.g. metallic thin films or etched semiconductor layers that are produced with the help of etching, with scanning probe tools or with nanolithography methods) or via combined methods where molecules are integrated into a top-down framework.

1.3   CNT Nanomotors

Nanomotors are nanoscale devices capable of generating linear and/or rotational motions. Even though the nanomotors available in nature exhibit exceptional power with reasonable efficiency, they lag behind when it comes to controllability and robustness. As a result, over the past few decades, a lot of physical principles (e.g. optical, thermal, electrical and chemical) have been developed to drive nanoscale motors [2, 6, 24-39, 43, 46]. Due to the exceptional mechanical [47] and electrical [9] properties CNTs are considered as a good candidate for nanomotors. CNTs are the stiffest material known, have low density, ultra

small cross-sections and can be fabricated with minimum defects [47]. In addition, a single nanotube can act as a transistor [13] and thus may be able to sense its own motion. The earliest CNT nanomotor was demonstrated by the Zettl group in 2003 using MWCNTs [28]. Other driving principles include driving nanomotors using thermal gradients, electron windmill etc. [24, 25, 40] The ability to be operated at a wide range of temperatures, pH and pressures are some of the advantages that make CNT nanomotors a better candidate than the rest of the nanomotors.

1.4   Literature Review

In literature different nanomotor driving principles such as optical [37], electrical [24, 28, 31], chemical [2, 48, 49], biological [38, 50, 51] means, have been reported. A large number of nanomotors rely on principles driven from biological mechanisms [38, 50, 51]. Among the few principles developed by the researchers, both linear and/or rotational nanomotors have been demonstrated. Linear nanomotors are the class of nanomotors realized by the linear motion of nanoparticles can be found in literature [25, 41]. The early experimental demonstration of these motors was illustrated by Barreiro *et al.* [25] and Somada *et al.* [41]. Barreiro *et al.* [25] used coaxial CNTs with a temperature gradient between the edges of one nanotube creating an imbalance in phonon distribution. Phonon imbalance generated by the thermal gradient in one nanotube triggered movement of the other tube. By using CNT capsules inside a host CNT, Somada *et al.* [41] was able to operate their linear nanomotor at around room temperature. More recently, Xu *et al.* [52] reported linear motion of hydrated nonpolar nanoparticles in presence of a nonuniform electric field. The nonuniform electric field produces an uneven distribution of water molecules around the nanoparticle forcing the

nanoparticle to move towards the weaker field direction in order to lower the total system energy.

Another extensively studied class of nanomotors relies on rotary motion of nanoparticles or nanostructures. Rotational nanomotors realized by different ways, such as optical [37], electrical [24, 28, 31], chemical [2, 48, 49], biological [38, 50, 51] means, have been reported. However, among the reported schemes, the numbers of nanomotor system driven by electrical energy are very few. [24, 28, 31] An early example of an electrically driven rotational nanomotor would be the system developed by Fennimore *et al.* [28]. This design involves a multiwall carbon nanotube (MWCNT) whose inner shell is free to rotate and outer shell is clamped to two metallic pads. A nanoscale metal pad is attached to the inner shell. The electrostatic interaction between the metallic plate and external gates is responsible for the inner shell rotation [28]. However, to accomplish rotation, three stator electrodes are also required by this system along with two electrically conducting anchors. The design requires complex fabrication procedure as well [31]. To obviate the need for metallic plate and other design complexities, Bailey *et al.* [24] has proposed a new drive mechanism – "electron-turbine" for MWCNT-based rotational nanomotor. Although they have theoretically shown that the drive mechanism originated from electron flux is sufficient to overcome frictional forces between the inner and outer tubes, rotating an external load with this design scheme is a matter of further investigation. More recently, Kim *et al.* [31] has reported a new design for the electrical energy driven rotary nanomotor system in deionized (DI) water which consists of multisegment Au/Ni/Au nanowires as rotators, tri-

layer Au/Ni/Cr magnets as bearings and quadruple microelectrodes as stators. It is apparent that this approach is also dependent on complex structures and assembling processes.

It is noteworthy that the applications of nanoscale systems associated with fluids in numerous physical, chemical, and biological systems have also got extensive attention in recent years [27, 31, 53]. For example, using molecular dynamics simulations, Wang *et al.* [53] has reported water molecules pumping by nanoscale propellers made of CNT and pyrene molecules (used as molecular-scale blades). However, they have not described explicitly about the motor system that may rotate the propellers. Using the aforementioned rotational nanomotor systems, driving external load such as molecular-scale blades or nano-gear based complex structures, especially in aqueous environment, might become difficult. No study on the performance of those systems in such environment has been reported. Although Kim *et al.* [31] has already reported nanowire rotation in DI water, the design lacks the facility to drive external loads. Altogether, an electrical energy driven nanomotor which is suitable to operate in water and capable of exerting enough force to rotate an external load has not yet been reported in literature. In addition, use of electric field induced water dipole orientations to drive NEMS, such as nonpolar CNT based nanostructures, is yet to be explored. The aim of this thesis is to propose such a nanomotor system, and analyze its characteristics.

1.5 Objectives of the Thesis

The objectives of this thesis are-

i.   To explore the effect of rotating electric fields on hydrated nanoparticles (such as CNT in water).

ii. Design a novel CNT-based nanomotor that utilizes the ultrafast orientation of hydrated nanoparticles due to the rotating electric field.

iii. Investigate the microscopic mechanisms and role of dipole behavior (such as dipole strength, orientation, energy variations etc.) in the operation of the designed nanomotor.

iv. Analyze the load driving capability of such nanomotors with molecular-scale loads (such as pyrene blades, gear-based complex structures etc.) attached to it.

v.   Study the precise angular control of molecular-scale loads (such as CNT).

1.6 Thesis Overview

This thesis is divided into four (4) chapters-

i.   Chapter 1 provides a general introduction followed by the background, literature review and objectives.

ii. Chapter 2 covers a brief description of the simulation methodology including theoretical overview and simulation modeling.

iii. In Chapter 3, we propose a novel nanomotor structure that makes use of the ultrafast orientation of hydrated nanoparticles guided by rotating electric fields. We also analyze the rotational characteristics of the proposed nanomotor along with its ability to drive molecular scale loads.

iv. Chapter 4 contains the concluding remarks followed by some suggestion on the possible future works.

Chapter 2

Theoretical Overview[1]

Due to the continuous growth in the field of nanotechnology, nanostructures such as Carbon nanotubes are becoming more and more important day by day. The importance of studying these structures in details is also increasing in a great pace. Hence the computer simulations of these structures are also becoming very popular these days. One interesting way to perform the simulation is the molecular dynamics simulation, where the physical movements of each atom are analyzed with respect to time. This method is used to investigate the structure, dynamics and orientation of nanostructures.

2.1   Molecular Dynamics (MD) Simulation

Molecular dynamics (MD) simulations are a class of atomistic simulation that is too complex for studying in analytical methods. While experiments provide with the most accurate descriptions of a specific phenomenon, they have intrinsic and practical limitations. Even though an analytical solution might provide a closer look into the underlying mechanism, it is often too involved, or sometimes, impractical. Another way of tackling the problem is to use different numerical techniques to solve the analytical equations using computer simulations. A very well-established method of solving the dynamics of atomistic systems is ab-initio simulations, where the Schrödinger equation is solved using the

---

[1] A version of this chapter has been published in a peer-reviewed journal (Reused with permission from "M. M. Rahman, M. M. Chowdhury, M. K. Alam, 'Rotating-Electric-Field-Induced Carbon-Nanotube-Based Nanomotor in Water: A Molecular Dynamics Study', Small, Wiley, vol. 13, pp. 1603978-1 - 1603978-10, 2017", Copyright 2017, John Wiley & Sons, Inc.).

positions of the nuclei and the number of electrons in order to yield useful information such as electron densities, energies and other properties of the system. However, carrying out the ab-initio simulation is very time consuming, when a large system is taken into account. Therefore, another well-established class of atomistic simulation, known as the molecular dynamics simulation, is frequently considered. In an MD simulation, we model the motion of a group of particles by solving the classical equations of motion. The atoms and molecules are allowed to interact for a period of time, giving a view of the motion of the atoms. This is accomplished by explicitly describing the atoms in the system as point masses, with the potential energy of the system being determined by a potential energy function. The trajectories of atoms and molecules are determined by numerically solving the Newton's equations of motion, with some quantum couplings. MD is frequently used to refine three dimensional structures of proteins and other macromolecules based on experimental constraints from X-ray crystallography or NMR spectroscopy. MD is also used to examine the dynamics of atomic-level phenomena that cannot be observed directly, such as thin film growth and ion-subplantation or nanostructures that have not been created yet.

In classical MD, atoms are given initial positions and velocities, and then forces on each particle are calculated by considering the influence of each of its neighbors. The Newtonian equations of motion are used to calculate the trajectories by allowing the particles to move under a constant force for a short time interval and then by recalculating a new force to apply for the next short time interval. For a system of N interacting particles

$$m_i \frac{\partial^2 r_i}{\partial t^2} = F_i, \ i = 1, 2, 3, ..., N, \tag{2.1}$$

Where, m_i is the mass of the particle, r_i its position, F_i the force acting on the particle, and t is the time. The force is derived from a potential function (force field) V using $F_i = -\dfrac{\partial V}{\partial r_i}$.

The structure to be analyzed is created using molecular visualization software (such as VMD, PyMol etc.) [54, 55] The energy of the entire system is minimized to achieve a relaxed structure. Then the initial positions and velocities of the relaxed structure are specified, and the forces are calculated using the aforementioned equations. The new coordinates and velocities are calculated, and this process is repeated until the specified time of the simulation is finished. This process is shown in the following flow chart.

```
                    ┌─────────────┐
                    │    START    │
                    └──────┬──────┘
                           │
                           ▼
              ┌────────────────────────┐
              │ Initialize Positions and│
              │       Velocities        │
              └────────────┬───────────┘
                           │
                           ▼
              ┌────────────────────────┐
          ┌──▶│  Calculate forces for all│
          │   │  molecules using Potential│
          │   └────────────┬───────────┘
          │                │
          │                ▼
  Till    │   ┌────────────────────────┐
Termination│  │  Apply Thermostat and   │
          │   │       Barostat          │
          │   └────────────┬───────────┘
          │                │
          │                ▼
          │   ┌────────────────────────┐
          │   │  Update Position and    │
          └───│       Velocities        │
              └────────────┬───────────┘
                           │
                           ▼
                    ┌─────────────┐
                    │Analyze Results│
                    └─────────────┘
```
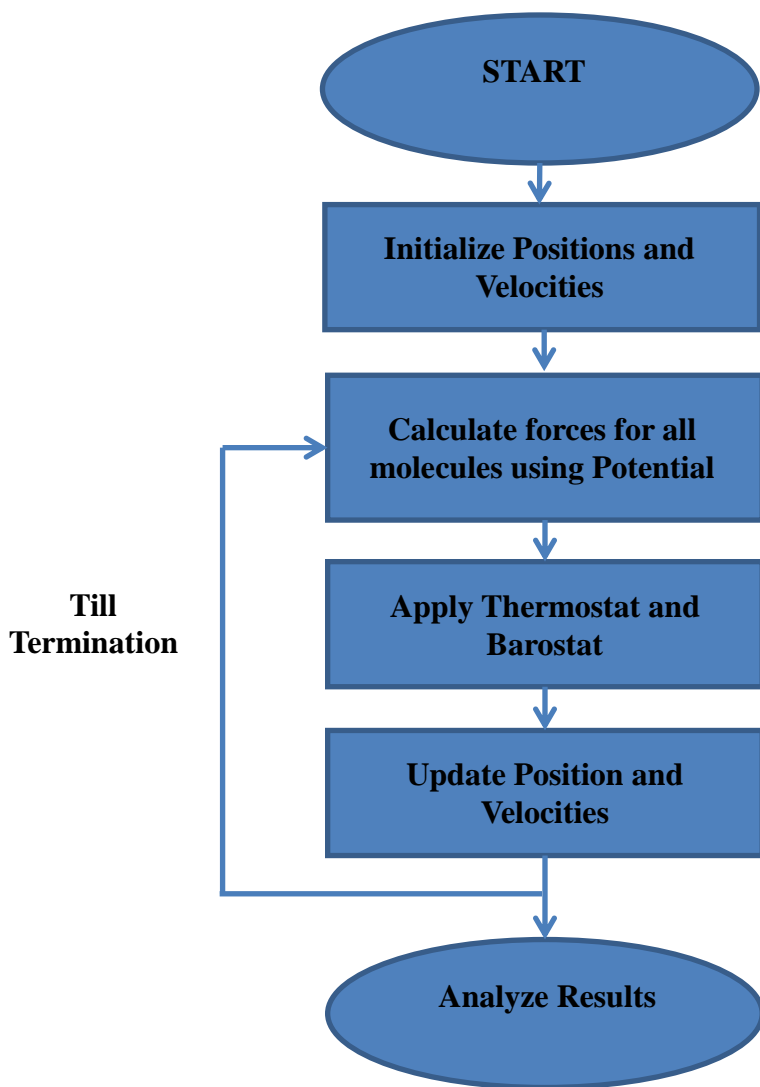
Fig. 2.1. Flow diagram of a molecular dynamic simulation.

2.1.1 Forcefield

In classical MD, forcefield refers to the functional form and parameters used to determine

the potential energy of a system of atoms [56-61]. It is one of the most fundamental aspects

of molecular dynamics simulations. The parameters of the energy functions may be derived

13

from experiments as well as analytical calculations in quantum mechanics [56, 61]. The basic functional form of a potential energy in molecular mechanics includes bonded terms for interactions of atoms that are linked by covalent bonds (such as H-O bonds present in water), and nonbonded terms that describe the long-range electrostatic and van der Waals forces (such as the weak interaction force between the 2 graphene layers in a graphite) [56, 61]. Therefore, the expressions of the energy terms are approximated as-

$$E_{total} = E_{bonded} + E_{nonbonded} \qquad (2.2)$$

$$E_{bonded} = E_{bond} + E_{angle} + E_{dihedral} \qquad (2.3)$$

$$E_{nonbonded} = E_{electrostatic} + E_{vdW} \qquad (2.4)$$

In addition to the functional form of the potentials, force fields define a set of parameters for different types of atoms, chemical bonds, dihedral angles etc. All interatomic potentials are based on many approximations, and derived from different types of experimental data. Thus, they are also termed as empirical forcefields. Some existing energy functions do not account for electronic polarization of the environment, an effect that can significantly reduce electrostatic interactions of partial atomic charges [56, 61]. Some of the most well-known forcefields are- AMBER, CHARMM, GROMOS, OPLS, REBO, ECEPP, AIREBO etc. [61]

2.1.2 Electrostatics

The electrostatics of an MD simulator is calculated using the Coulomb's expression [61]. However, the direct sum of Coulombic equation to calculate the electrostatics is considered tedious and computationally expensive compared to other numerical techniques such as

Particle Mesh Ewald (PME) [56]. PME is considered as a faster method to compute energies or forces than the conventional methods [56]. It splits the direct sum expression into two series, the fast variation art for small and large radii. The small radius terms decay fast and become negligible beyond a cutoff distance. Since the long range interaction cannot be computed by a sum in real space directly, the series is then Fourier transformed, and solved for using standard FFT techniques [61].

2.1.3 Temperature and Pressure Bath (Thermostat and Barostat)

Thermostats and barostats are designed to help a simulation sample from the correct ensemble (*i.e.*, NVT or NPT) by modulating the temperature and pressure of the system [56]. In simulations, the instantaneous temperature is usually computed from the kinetic energy of the system using the equipartition theorem. In other words, the temperature is computed from the system's total kinetic energy. The thermostat keeps the average temperature of a system constant. Some of the most common thermostats are Berendsen, Nosé–Hoover etc. In case of pressure, the system pressure is set toward a desired value by changing dimensions of the simulation cell size during the simulation [56]. Some of the most common barostats are Parrinello-Rahman, Berendsen etc.

2.1.4 Boundary conditions

Since the length-scale of MD is limited, a large fraction of the atoms remains on the surface, and are affected by presence of the surface. Several boundary conditions are used to consider this artifacts caused by the limited size of the system [56]. Some of the most

common boundary conditions are Free, Rigid, Periodic etc. While the Free and rigid boundary conditions are good approximations for molecules placed in a vacuum, Periodic boundary conditions (PBCs) are useful for approximating the behavior of macro-scale systems of gases, liquids, and solids. Three-dimensional PBCs can also be used to simulate planar surfaces, in which case two-dimensional PBCs are often more suitable. PBC is also chosen for approximating a large (even infinite) system by using a small part called a unit cell [56, 58, 66].

2.2 Models and Simulation parameters

In this study, we use molecular dynamics (MD) simulations to investigate the rotational characteristics of the proposed nanomotor. GROMACS 4.6.5 package [56] was used to perform all the simulations. The OPLS-AA forcefield [57] was employed and the carbon atoms were considered as uncharged Lennard-Jones (LJ) particles and described by a combination of bonded as well as nonbonded interaction potentials. While the bonded interactions were modeled by a Morse bond potential for stretching, a harmonic cosine potential for bending and a twofold cosine potential for torsion, the nonbonded interaction included a Lennard-Jones (LJ) 12-6 potential [17, 46, 58-60]:

$$U(\mathrm{r}_{ij},\theta_{ijk},\varphi_{ijkl}) = K_{Cr}[\exp(-\gamma(\mathrm{r}_{ij}-\mathrm{r}_C))-1]^2 + \frac{1}{2}K_{C\theta}(\cos\theta_{ijk}-\cos\theta_C)^2 + \frac{1}{2}K_{C\varphi}(1+\cos(2\varphi_{ijkl}-\varphi_C))$$

$$+4\varepsilon_{CC}\left[\left(\frac{\sigma_{CC}}{r_{ij}}\right)^{12}-\left(\frac{\sigma_{CC}}{r_{ij}}\right)^6\right], \tag{2.5}$$

where, the bonding parameters K_{Cr}, r_C and γ are the parameters for the Morse bond potential; $K_{C\theta}$ and θ_C are the parameters for the bending angle potential; $K_{C\varphi}$ and φ_C are the torsion parameters. The nonbonded parameters ε_{CC} and σ_{CC} are the LJ interaction for carbon-carbon interactions [17, 46, 58-60]. As proposed by Jorgensen *et al.*, [57] the bonds, angles, dihedrals and nonbonded potential terms of the OPLS-AA forcefield are simply additive. The bonded potential terms are commonly limited up to 4-body interactions, where the higher body interactions can be ignored [61]. The nonbonded potential contributions are excluded from these interactions and suitable functional forms (e.g. LJ 12-6 potential in this case) are added separately for simplicity [57]. The values of the interaction potential parameters for carbon atoms are given in Table 2.1.

Table 2.1. Parameters for interaction potentials used in the simulations

Interaction potential parameters	
$K_{Cr} = 478.9$ kJ mol^{-1}	$r_C = 0.1418$ nm
$K_{C\varphi} = 25.12$ kJ mol^{-1}	$\gamma = 21.867$ nm^{-1}
$K_{C\theta} = 562.2$ kJ mol^{-1}	$\theta_C = 120°$
$\varepsilon_{CC} = 0.3601$ kJ mol^{-1}	$\varphi_C = 180°$
	$\sigma_{CC} = 0.3400$ nm

In case of the water molecules, the TIP3P water model [62] has been used. The CNT-water interactions have been described by a Carbon-Oxygen LJ potential [58]. The values of ε_{CO} and σ_{CO} have been chosen to be 0.4787 kJ mol^{-1} and 0.3275 nm, respectively. It can be noted that the interaction potential employed in the present study is commonly used in predicting the dynamics of CNT based systems with a variety of other molecules such as water, ethanol, DNA, lipids, amino acids etc. [58, 60, 63-66] It is also in a good agreement with the experimental properties of water [57, 62]. Moreover, the potential is very consistent for a wide range of temperature variation [67-69]. The CNT-water interactions have been described by a Carbon-Oxygen LJ potential [17, 46, 58, 59, 66, 70]**:**

$$U(\mathbf{r}_{ij}, \theta_{ijk}) = \frac{1}{2} K_{Wr} (\mathbf{r}_{ij} - \mathbf{r}_W)^2 + \frac{1}{2} K_{W\theta} (\cos\theta_{ijk} - \cos\theta_W)^2, \quad\quad\quad (2.6)$$

where, r_W and θ_W are the reference O-H bond length and H-O-H angle, and the K_{Wr} and $K_{W\theta}$ are the corresponding force constants. The well-established TIP3P water model has been used to represent water molecules. The values of the interaction potential parameters for water are given in Table 2.2.

Table 2.2 Parameters for the TIP3P Water Model

Interaction Potential Parameters	
$K_{Wr} = 502416$ kJ mol^{-1}	$r_W = 0.09572$ nm
$K_{W\theta} = 628.02$ kJ mol^{-1}	$\theta_W = 104.52°$
$\varepsilon_{OO} = 0.6367$ kJ mol^{-1}	$\sigma_{OO} = 0.3151$ nm
$q_O = -0.834e$	$q_H = 0.417e$

To obviate the problems with the dangling bonds, hydrogen atoms have been covalently attached to the edges of the CNTs. The simulations were carried out at a constant temperature (300 K) and pressure (1 bar) unless mentioned otherwise. For this purpose, the Nose–Hoover thermostat [71] and the Berendsen barostat [72] were used with a coupling time of 0.1 and 1.0 ps accordingly. The equations of motion were solved using the Leap-frog integration scheme with a time step of 2 fs. A cut-off radius of 1.2 nm for the Lennard-Jones interactions was used. The long-range electrostatic interactions were calculated using the Particle-Mesh Ewald (PME) method [73]. To keep the total number of atoms constant, periodic boundary condition was applied in all directions [17, 46, 58, 59, 66, 70]. To achieve a structure with a natural orientation, energy minimization was performed. The molecular graphics program VMD 1.9.1 was used for visualizing and analysing MD trajectories [54].

GROMACS uses the leap-frog algorithm [56] to integrate the Newtonian equations of motion. It uses positions r at a time t and velocities v at time $(t - \Delta t/2)$; it updates positions and velocities using the forces $F(t)$ determined by the positions at time t using

$$v(t+\frac{\Delta t}{2}) = v(t-\frac{\Delta t}{2}) + \frac{F(t)}{m}\Delta t \qquad (2.7)$$

and

$$r(t+\Delta t) = r(t) + v(t+\frac{\Delta t}{2})\Delta t \qquad (2.8)$$

The leap-frog scheme is a modification of the Verlet scheme [56]. The error in the positions calculated through the unmodified Verlet scheme is on the order of $(\Delta t)/2$, while the leap-frog scheme results in a global error of the order $(\Delta t)/3$ thus providing more accurate predictions of the positions and velocities of the atoms for the same time step. The time step Δt used for integration is of critical importance to the accuracy of MD simulations. A value of Δt that is too large will lead to an unstable system and a drift in the total energy of the system, while a value that is too small will increase the time of the simulation and the size of the output files drastically. In principle, the time step is governed by the largest oscillation frequency in the system. This is in general associated with the hydrogen atoms in the system. The leap-frog integrator used in GROMACS allows a maximum time step of 2 fs without compromising the accuracy of the simulations [56]. The time step used in the simulations presented in this thesis was 2 fs for all simulations. Even though the time varying electric field can be applied in GROMACS 4.6.5 package, application of a rotating electric field around a plane is not incorporated in GROMACS. Therefore, the source code

of GROMACS 4.6.5 package was modified to be able to simulate a rotating electric field. The source code was also modified to emulate the application of space dependent electric field (*i.e.* E-field applied only to a specific portion in the simulation box).

Chapter 3

Results and Discussion[2]

3.1 Design and Principle of Operation

3.1.1   Principle of Operation

When a nanoparticle is immersed in water under the influence of a static electric field, it gets oriented toward the applied field [66, 70]. The dynamics of this alignment process has been discussed by Daub *et al.* [70] All dipolar fluids have a tendency to arrange their dipoles parallel to both the nanoparticle interface as well as the applied field. Therefore, the nanoparticle is induced to align its interface with the field [66, 70]. This orientation mechanism has been studied rigorously for single walled CNTs by Guo *et al.* [66] using MD simulations. According to Guo *et al.*, [66] when we apply an electric field, water molecules orient toward the field direction due to their dipoles, and also try to orient parallel to the surface of CNT in order to maximize hydrogen bonds. To satisfy these two requirements, the CNT is forced to orient its surface toward the electric field. [66] Thus, we first investigated whether it is possible to use the orientation mechanism for rotating a CNT, by placing it in a rotating electric field. For this purpose, we placed a (10, 0) CNT of length 4.01 nm in a 7.5 nm×7.5 nm×7.5 nm cubic box containing about 41,000 water molecules and applied a rotating electric field of 1.0 V/nm magnitude and 1.5×10^{11} r.p.m. angular

---

speed. It can be noted that unlike the rotation of nanowires reported by Fan *et al.*, [27] where the rotation of CNT was achieved experimentally due to the polarization of CNT, we show that only the water dipole orientations are sufficient to rotate a CNT suspended in water. The rotating electric field can be realized using quadruple electrodes [27]. In practical cases, when the CNT will be hundreds of nanometers in length, which is obtainable in an experiment, the required field strength may be reduced significantly [66]. The schematics in Figure 3.1 show the CNT at different angular displacements (see supplementary movie 1 of Ref 46[3]). Thereby, the CNT is successfully 'locked' with the electric field and follows the rotation of the applied electric field of particular magnitude and angular speed.
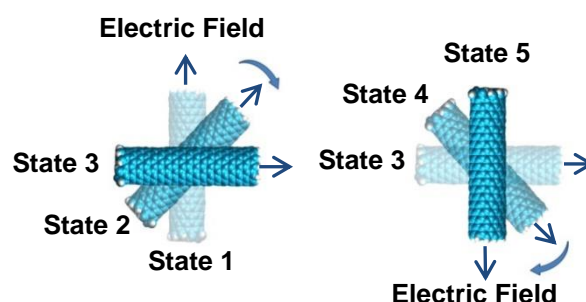
Figure 3.1. Series of images showing the CNT at different angular displacements. An applied electric field forces the CNT to orient towards the field direction. States 1 to 5 demonstrate the CNT rotation along with a rotating electric field. The straight arrows show the applied electric field directions. Water molecules are not shown for clarity.

3.1.2 Design of the Nanomotor

To utilize the CNT rotation in nanomotor application, we have developed a particular configuration as shown in Figure 3.2. Figure 3.2(a) shows a simplified schematic representation of the proposed nanomotor while Figures 3.2(b) and 3.2(c) represent the

---

[3] http://onlinelibrary.wiley.com/wol1/doi/10.1002/smll.201603978/suppinfo

corresponding structure in atom based schematics. Two 'wing CNTs' of chirality (6,0) and length 0.85 nm which work as the motor shaft, are attached with a larger (14,14) 'central CNT' of length 3.84 nm. The wing CNTs are kept inside the two 'fixed CNTs' of chirality (8,8) and length 0.37 nm. These fixed CNTs work as a support for the rotating wing CNTs. In practical cases, the fixed CNTs will be attached to some rigid supports. In our simulations, we fixed only 6 atoms from the bottom of each 'fixed CNT' to mimic the scenario of a CNT placed on a rigid substrate. One wing CNT's length is made longer than its corresponding fixed CNT so that a segment of it becomes uncovered and a load can be attached to it. The diameters of the wing and fixed CNTs have been chosen carefully. The wall to wall distance (*i.e.*, the radius difference between wing and fixed CNTs) cannot be made less than the collision diameter of carbon atoms, otherwise, the system will become unstable [58]. On the other hand, if we make the wall to wall distance too large, there will be considerable amount of water molecules in the inter-tube region which is not desirable in this case. In total, the nanomotor configuration has been made in such a way that the wing CNTs do not come in contact with considerable amount of water molecules whereas the central CNT is fully exposed to its surrounding water molecules. When we apply an electric field, the central CNT aligns itself toward the field due to the presence of water molecules around it (see supplementary movie 2 of Ref. 46[4]). In contrast, the wing CNTs do not align toward the field, since they are inside the fixed CNTs and experience small number of water molecules around them. Therefore, we can attach load to the wing CNT which works as the motor shaft. Unlike any other previous electrical energy driven nanomotors [24, 28, 31], availability of a rotating shaft to connect load is a unique feature of the proposed nanomotor scheme.

---

[4] http://onlinelibrary.wiley.com/wol1/doi/10.1002/smll.201603978/suppinfo
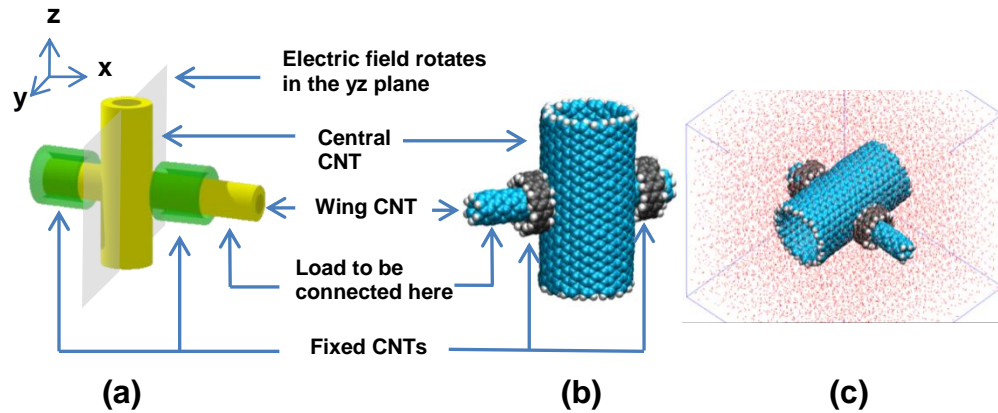
Figure 3.2. The proposed nanomotor configuration. (a) Simplified schematic representation (not drawn to scale). (b) Corresponding atom based structure. (c) Nanomotor structure immersed in DI water.

To prepare a junction among CNTs, different tools and methods are used, e.g. electron beam irradiation or ion irradiation, mechanical manipulation with atomic force microscope, nanotube soldering, chemical functionalization, heat welding etc. Using these techniques, synthesis of 'X', 'Y', 'T', 'H' junctions have been reported in literature [46, 47]. Synthesis of crossed junction CNTs has also been studied widely. In general, controlled electron beam irradiation technique is used to prepare crossed junction CNTs. After preparing the crossed junction CNTs, bottom-up self-assembly process can be used to develop the whole structure [Figure 3.2(a)]. In another way, at first, electrical breakdown technique can be applied to remove the central portion of the outer tube of a multiwall CNT [46, 47]. Afterwards, controlled electron beam irradiation technique can be used to prepare the crossed junction CNT at the middle portion of the inner tube as mentioned above [46, 47].

In recent years, application of nanomotor in drug-delivery has also received an extensive attention. Kim *et al.* [6] has discussed and studied in detail about their nanomotor's application for drug-delivery. They have mentioned that their motor contains non-biocompatible materials, such as Ni in multisegment nanowires and magnetic bearings, which are required to be replaced by any other biocompatible magnetic materials. On the other hand, our proposed structure does not contain any non-biocompatible materials. In addition, it does not require any complex structures, such as magnetic bearings or multisegment nanowires as well. Furthermore, Kim *et al.* [31] has reported 15 hours duration time for their micromotor. After 15 hours of rotation, a layer on magnetic bearing was significantly thinned by frictional wearing and the motor operation was stopped eventually. Later on, Guo *et al.* [29] improved their micromotor longevity to 80 hours, which is the highest duration time for a nano/micromotor made from synthesized nanoparticles by using a more wear-resistant material between the rotor and the bearing. On the other hand, the proposed nanomotor does not go through any frictional wearing except for the intershell friction between the arm and fixed CNTs. As the intershell friction of MWCNTs is ultralow in nature (less than 1 nN), [58] the proposed system is expected to have a lower frictional wear and hence a longer durability.

3.2 Characterization of the proposed Nanomotor

3.2.1. Analysis of the Rotational Characteristics

When we apply a rotating electric field at the central CNT, it starts to rotate along with the wing CNTs (see supplementary movie 2 of Ref. 46[5]). For a successful rotation, the central CNT is required to exert enough force which overcomes the frictional forces between the fixed and wing CNTs. The rotation of the system implies that the electric field induced revolving central CNT can be used to rotate an external object attached to the wing CNTs as loads.
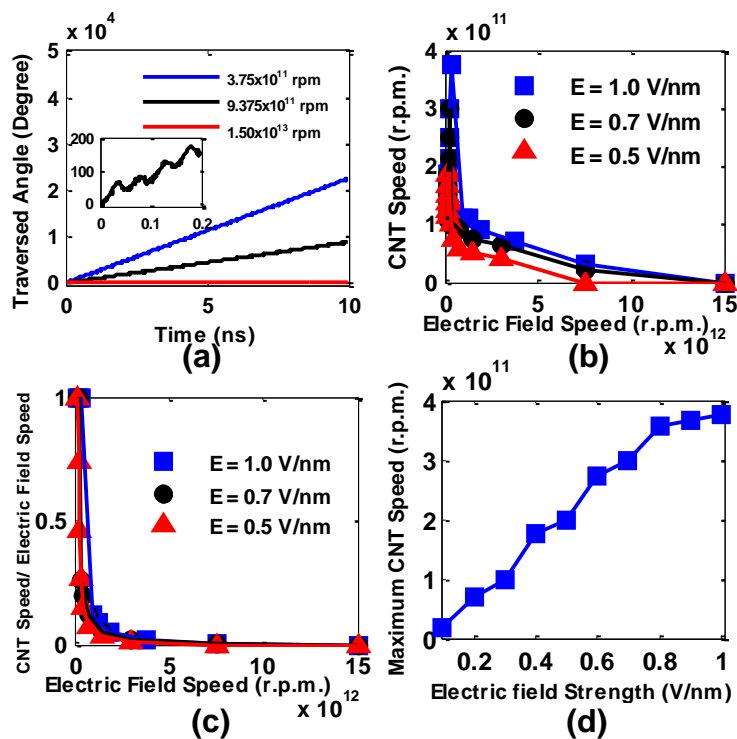
Figure 3.3. (a) History of traversed angle of the nanomotor for an applied electric field of 1.0 V/nm at three different frequencies. (b) Effect of electric field speed and strength on the speed of the nanomotor. (c) The ratio of CNT speed to electric field speed against the electric field rotation speed. (d) Effect of field strength on the maximum speed of the nanomotor.

---

[5] http://onlinelibrary.wiley.com/wol1/doi/10.1002/smll.201603978/suppinfo

Figure 3.3(a) shows the traversed angle of the nanomotor with respect to time for 3 different electric field rotational speeds having a fixed strength of 1.0 V/nm. The central CNT can follow the electric field at 3.75×10^{11} r.p.m. Therefore, the motor remains 'locked' to the applied field [Figure 3.3(a), blue curve]. However, the central CNT cannot keep up with the electric field at an arbitrarily high frequency. For instance, if the applied field is increased to 9.375×10^{11} r.p.m., the central CNT follows the electric field with a combination of forward and backward motions [Figure 3.3(a), black curve]. It takes a finite amount of time for water dipoles to align the central CNT towards the applied field. When the field is changed faster than that period, central CNT cannot continuously follow the direction of electric field. Hence the motor performs 'interrupted' rotations [see the inset of Figure 3.3(a)]. For an even higher speed (1.5×10^{13} r.p.m.), the central CNT is totally unresponsive to the applied electric field because the field frequency is too fast for the CNT to follow. In this case, no angular rotation can be achieved from the motor [Figure 3.3(a), red curve].

In Figure 3.3(b), we show the effect of electric field speed and strength on the speed of the nanomotor. For this purpose, we have calculated the speed of rotation at different frequencies for the field strengths of 1.0, 0.7 and 0.5 V/nm. The frequencies were varied from 1×10^{11} r.p.m. to 1.5×10^{13} r.p.m. Our results show that higher rotational speed can be attained at higher field strengths. In Figure 3.3(c), we present the ratio of CNT rotation speed to electric field rotation speed and show that such ratio dramatically drops down to zero at higher field speeds. Figure 3.3(d) shows the maximum speed of the nanomotor for different field strengths (0.1 to 1.0 V/nm). Indeed, the motor can be operated at any speed

below the maximum speed simply by adjusting the speed of the rotating field. The reasons behind such characteristics can be understood from the response behavior of water dipole at different field speed and strength (discussed in section 3.2.2). Moreover, a critical value of electric field strength is expected to exist below which no actuated rotation would occur. However, the critical field strength is also dependent upon the CNT parameters (length and radius). For our simulated case of a (14,14) CNT of length 3.84 nm, no actuated rotation was observed for an external field strength of 0.06 V/nm within a total simulation time of 10 ns.

In literature, the response time of water under electric field has been reported to be ultrafast in nature [74]. Therefore, the water dipole orientation is found to be synchronous with the electric field rotation within the operating range of the proposed nanomotor (up to 1.5×10^{13} r.p.m.). However, in general, the CNT rotation is not synchronous with the water dipole rotation. For sufficiently low rotational speeds, the CNT rotation might be almost synchronous, whereas at higher speeds (up to the maximum speed), there exists a certain angular lag between the water dipole orientation and the CNT. Figure 3.4(a) shows the traversed angle of the water dipoles and the CNT at a field strength of 1 V/nm and speed of 3.75×10^{11} r.p.m. A clear lag angle of about 34º (15 ps of time lag) is observed between the net water dipole and the CNT. If an electric field having higher rotational frequency than the maximum attainable CNT speed is employed, the lag angle can no longer be constant and the motor shows a combination of forward and backward motions. Figure 3.4(b) shows the traversed angle of such motion of the CNT for an applied field of 1V/nm and speeds of 6.25×10^{11} and 9.375×10^{11} r.p.m. The mechanism is clearly illustrated in Figure 3.4(c) (see

supplementary movie 3 of Ref 46[6]). As the rotating electric field advances, the lag angle continues to increase [Figure 3.4(c), 228 to 256 ps]. However, when the lag angle becomes greater than 90º, the CNT is forced to rotate in the opposite direction to align itself to the opposite end of the electric field due to its nonpolar nature [Figure 3.4(c), 260 ps and 275 ps]. Therefore, the CNT moves counterclockwise. However, at 300 ps, the electric field crosses the CNT again enabling it to resume its clockwise motion. Thus, the CNT makes a combination of forward and backward movements periodically throughout the entire simulation.
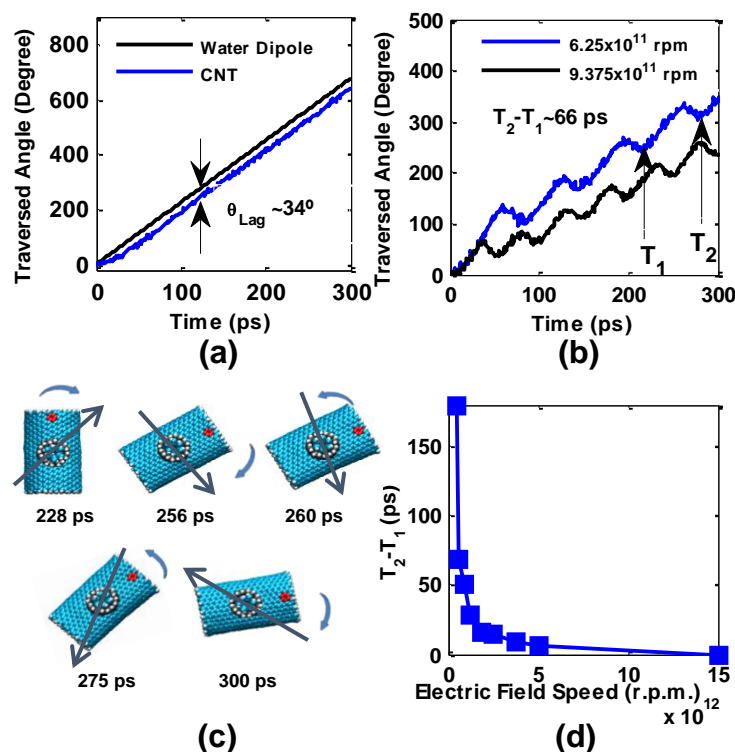
Figure 3.4. (a) History of traversed angle of the net water dipole and the CNT at an external field strength of 1V/nm and rotational speed of 3.75×10^{11} r.p.m. (b) History of traversed angle of the CNT at 6.25×10^{11} and 9.375×10^{11} r.p.m., where the CNT performs a combination of forward and backward motions. (c) Illustration of the forward and backward motions of the central CNT of the nanomotor. The direction of the electric field is indicated by an arrow.

---

6   http://onlinelibrary.wiley.com/wol1/doi/10.1002/smll.201603978/suppinfo

Figure 3.4(b) shows that this time period ($T_2 - T_1$) is about 66 ps for a rotational electric field speed of 6.25×10^{11} r.p.m. As expected, the higher the frequency of the rotating field, the lesser time the CNT gets to orient itself towards the field. Thus, ($T_2 - T_1$) drops to ~51 ps at an even higher rotational field speed of 9.375×10^{11} r.p.m. [Figure 3.4(b)]. Figure 3.4(d) shows the variation of ($T_2 - T_1$) with electric field rotational speed. Indeed, such time period drops down to zero as the frequency of the field is increased. This also explains the rotational behavior of nanomotor shown in Figures 3.3(a) and 3.3(b). For example, speed of the rotating field is so high for the case of red curve in Figure 3.3(a) that the field traverses an angle of 180º before the CNT could produce any angular advancement. Thus, ($T_2 - T_1$) drops to zero and the motor has no actuated rotation. Moreover, the net water dipole strength decreases at higher electric field speed (discussed in the next section). Therefore, at higher electric field frequencies, rotation of the motor drops to zero because of twofold actions-decrease of the net dipole moment and decrease of the forward and backward motions time period due to the lagging behavior.

It can be mentioned that Santamaría-Holek *et al.* [40] demonstrated a CNT-based nanomotor by utilizing the inhomogeneity of phonon distribution in CNT due to an external thermal gradient. To investigate whether a thermal gradient in the liquid can affect the performance of the proposed nanomotor, we simulated different combinations of thermal fluctuations in the liquid. The nanomotor was found to operate at higher rotational speed with an overall increase of the system temperature because of the decreased viscous dragging torque [31]. However, a thermal gradient, if present in the system, would affect the system differently depending on its direction. In our case, an overall decrease of the speed was observed under

the presence of a thermal gradient applied along the rotational plane (YZ). For instance, the central CNT remains 'locked' to an applied field strength of 1 V/nm and speed of 3.75×10^{11} r.p.m. without any thermal gradient. However, the speed drops to 1.6×10^{11} r.p.m. in presence of a thermal gradient of about 10^9 K/m along the Y axis. It has been reported that transport of fluid can also be achieved using a thermal gradient [75]. In addition, according to Bresme *et al.* [76], thermal gradient polarizes water in the direction of the gradient, leading to a non-negligible electrostatic field. The drop of speed found in our analysis in presence of a thermal gradient could be a combinational result of the above mentioned effects.

Furthermore, to show that the general conclusions drawn from the simulations are not limited to smaller sized CNTs, simulations were carried out with longer CNTs (supplementary movie 4 of Ref. 46[7] for a 15.39 nm central CNT, 1.85 nm wing CNTs and 0.98 nm fixed CNTs at a field strength and speed of 1 V/nm and 0.625×10^{11} r.p.m., respectively). The simulations show that the proposed driving principle can be applied to larger structures as well. Since longer CNTs would require significantly increased simulation box, smaller sized CNTs have been considered in most of the simulations to save computational time. It is also important to mention that longer central CNTs increase the total system inertia and consequently decrease the maximum speed of operation (a maximum speed of about 0.625×10^{11} r.p.m. was observed for the nanomotor having 15.39 nm central CNT).

---

[7] http://onlinelibrary.wiley.com/wol1/doi/10.1002/smll.201603978/suppinfo

3.2.2. Role of the water dipole orientations

Next, we analyze the microscopic behavior of the rotational actuation due to water dipole orientation. When a rotating field is applied in the YZ plane, electric field in the Y and Z directions is varied sinusoidally with a 90º phase difference between them. The water dipoles tend to align with the resultant electric field. Therefore, the average water dipole strengths along X, Y and Z axes (p_x, p_y and p_z respectively) vary in the same way as the electric field in their respective directions [Figure 3.5(a)]. Stronger electric field induces higher degree of orientation in water dipoles. Thus, the net average dipole strength increases at higher field strengths [Figure 3.5(b)]. Since the net dipole strength is also affected by the frequency of the rotating field [Figure 3.5(c)], we used a constant rotating field frequency (1.5×10^{11} r.p.m.) to observe only the effect of electric field strength in Figure 3.5(b). At higher electric fields, most of the water dipoles become aligned and the average dipole moment starts to saturate. A complete orientation towards the electric field would correspond to a net dipole moment of 2.35 D [77]. Figure 3.5(c) shows the water dipole moment strength vs. electric field speed behavior for a constant field strength of 1.0 V/nm. As reported in literature, water molecules have a finite response time to the applied field.[55] At lower frequencies, the dipoles can easily follow the rotating field which corresponds to the relatively flat section of Figure 3.5(c). However, at higher frequencies, the water dipoles get less time to respond to the field and therefore, the net average dipole strength decreases.
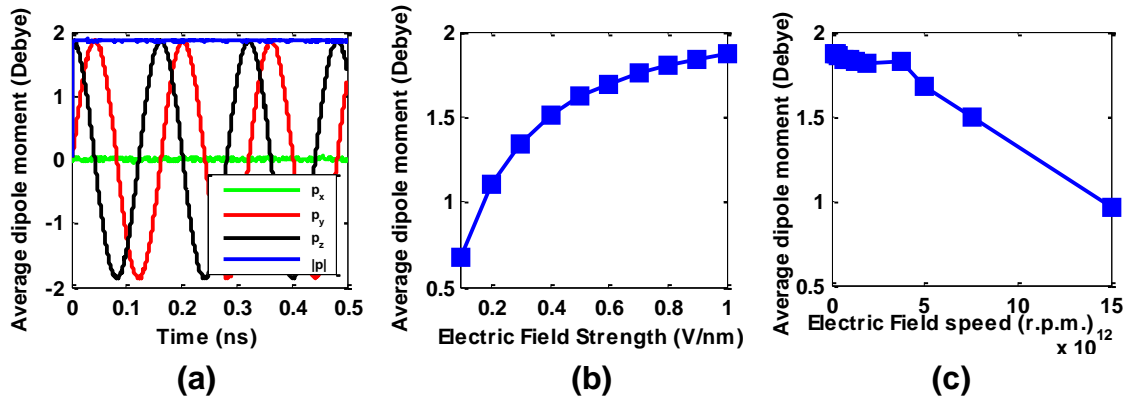
Figure 3.5. Variation of the water dipole orientation with the electric field. (a) Variation of the average dipole strength along x, y and z directions for a field strength of 1 V/nm and speed 3.75×10^{11} r.p.m. (b) Effect of field strength on the net average water dipole strength at a constant frequency of 1.5×10^{11} r.p.m. (c) Effect of electric field rotational speed on the net average dipole strength at a constant field strength of 1.0 V/nm.

Since the entire setup is immersed in water, question may arise whether a rotating CNT induces a motion and creates a local vorticity in the water. In our case, it is the orientation of the water molecules' dipole that causes the motion of the CNT. Therefore, no such hydrodynamic effects are expected to occur. It can be noted that previous experimental studies on rotating nanowires suspended in water have not also reported the presence of any such effects [6, 27, 31]. To confirm this in the present scenario, we applied a rotating field (1.0 V/nm, 3.75×10^{11} r.p.m.) to the nanomotor for 500 ps. Then, we stopped the field and simulated the system for another 500 ps. Since the water dipole relaxation process is ultrafast in nature [74], effect of the external field on water dipoles is expected to disappear within a very short period. Indeed, this phenomenon is confirmed by Figure 3.6(a). For further insight, we analyzed the trajectories of water molecules and found that they are always random. Figure 3.6(b) shows the angular position of 4 water molecules (fewer molecules are shown for clarity) along the YZ plane, randomly chosen from the system. As

33

can be seen from Figure 3.6(b), the molecules' trajectories are of random nature both in presence and absence of the electric field.
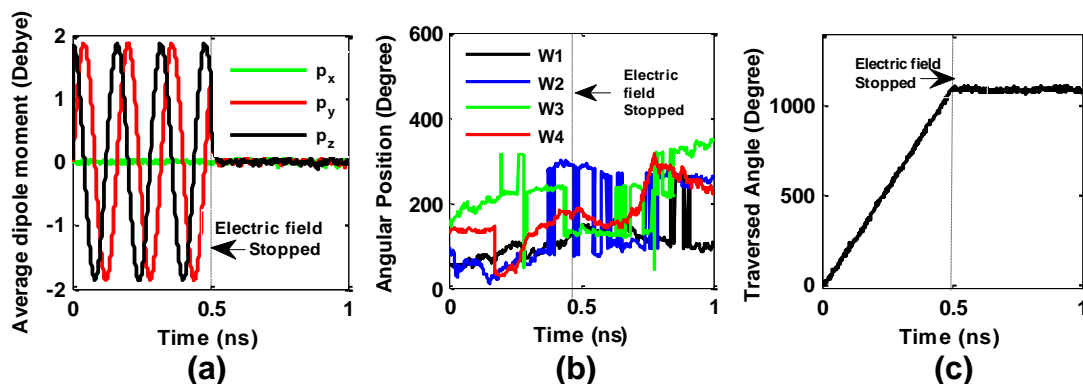

Figure 3.6. Response of water dipoles and nanomotor when the electric field is stopped abruptly at 500 ps (a) Average water dipole moments in the x, y and z directions. (b) Angular position of four randomly chosen water molecules along the YZ plane. (c) Traversed angle of the nanomotor.

The abrupt angular transitions in Figure 3.6(b) are the result of periodic boundary condition. It is widely employed in simulating systems immersed in liquids and mimics practical scenario [17, 58, 59, 66, 70]. In this case, each time a water molecule leaves the simulation boundary, an identical water molecule enters into the system from the opposite end to ensure the simulation of a constant number of atoms. The important fact to observe is that no molecule shows an angular advancement of 360° in presence of the electric field during its entire trajectory (one cycle period=160 ps). Thus, only the dipole orientation (under electric field) is responsible for rotating the CNT. In supplementary movie 5 of Ref 46[8], we show the trajectories of these water molecules along with the nanomotor structure which also confirms the nonexistence of any vorticity effect. One important point to notice is that the dipole moments p_y and p_z start to drop immediately when the field is absent [Figure 3.6(a)]. Therefore, the 90º phase difference between these two dipole moments is immediately

---

[8] http://onlinelibrary.wiley.com/wol1/doi/10.1002/smll.201603978/suppinfo

broken and no rotating net dipole moment of the water molecules is present. However, a closer look into Figure 3.6(c) reveals a small advancement (~12º) of the CNT after the removal of applied field. This insignificant motion can be attributed to the inertia of the rotating CNT which is diminished by the impedance of the water molecules within a very short period of time (~11 ps).

Rinne *et al* [77] reported pumping of water along CNTs with the aid of electrodes having charges oscillating in gigahertz frequencies. According to their microscopic theory based on a polarization-dragging mechanism, the oscillating charges produce a spatiotemporal structure of the field along the CNT axis which corresponds to a wave package with a finite phase velocity [77]. Therefore, the water molecules are polarized and dragged along the CNT axis in their case. However, in the present condition, no such effect is likely to occur since the magnitude of electric field is the same throughout the entire simulation box with only its direction changing with time. Indeed, the water dipoles are continuously orienting with the rotating field without being dragged by any spatial electric field gradient. Had the water molecules been dragged by the electric field to perform a circular motion, we would have expected a vorticity created inside the water. However, as mentioned before, our simulation shows no such motion is created inside the water [Figure 3.6(b) and see supplementary movie 5 of Ref 46[9]].

Next, we show the energy variance of the CNT-water nanomotor system when the field is rotated. Figure 3.7(a) shows that the system energy decreases as a rotating electric field is applied. A decrease in energy indicates the preferential orientation of water molecules

---

[9] http://onlinelibrary.wiley.com/wol1/doi/10.1002/smll.201603978/suppinfo

around the CNT. This phenomenon was also observed by Guo *et al.*, [66] where a higher water density in the first hydration shell along the CNT axis was observed at higher field strengths. Thus, stronger electric field induces higher degree of orientation of water molecules around the CNT and therefore lowers the total system energy [Figure 3.7(b)]. It can also be noted that similar behavior on the effect of electric field on hydrated nanoparticles has been observed by Winarto *et al.* [64] However, at higher frequencies, the water molecules get less time to orient around the CNT (as mentioned above) and the system energy increases with the electric field rotating speed [Figure 3.7(c)].
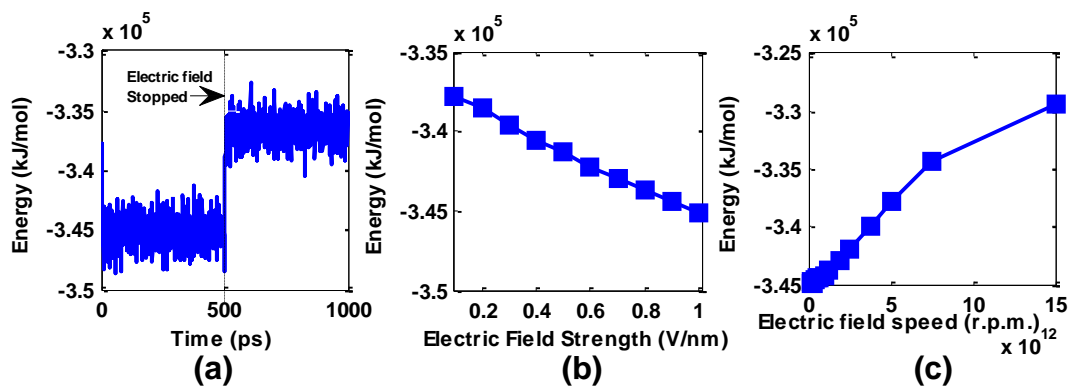
Figure 3.7. Variation of total energy of the nanomotor system with a rotating field (1V/nm, 3.75×10^{11} r.p.m.). (a) History of total energy of the system when the electric field is removed at 650 ps. (b) Effect of field strength on total energy of the system. (c) Effect of electric field speed on total energy of the system.

3.2.3.   Nanomotor with external loads

We have also investigated whether the nanomotor system can exert enough force to rotate molecular-scale blades [53] attached to it. We connected three Pyrene molecules with the wing CNT which work as molecular-scale blades [Figure 3.8(a)]. In practical cases, this system could be realized by cyclic addition reactions [47, 53]. One important thing to

mention here is that the electric field has only been applied inside the region within the two fixed CNTs (no electric field has been applied in the load region). Otherwise, the load itself will be affected by the applied electric field. For a successful rotation, the system not only has to overcome the friction of the fixed and wing CNTs but also the moment of inertia of the attached load and the interactions of blades with water molecules. Our results show that the motor can rotate along with three pyrene molecules attached as loads (see supplementary movie 6 of Ref. 46[10]). However, the maximum motor speed is reduced to 3.35×10^{11} r.p.m. in this case for an electric field of 1.0 V/nm. This ultrahigh speed is originated from the fast responsiveness of CNT orientation in water [66, 70]. It is important to mention that Daub *et al.* [70] has also reported very fast alignment (in pico-second range) of nanoparticle suspended in water along the applied electric field. In this work, we have thoroughly investigated the capability of our proposed nanomotor to rotate external mechanical loads. Figure 3.3(b) implies that the rotation speed of central CNT can be successfully controlled by the applied field. This controlled speed could be utilized in the fields of controlled biochemical release [31, 78] and drug delivery [79, 80]. Also, as reported by Wang *et al.* [53], pumping of water can also be achieved by attaching suitable configurations of pyrene molecules to the shaft of the nanomotor.
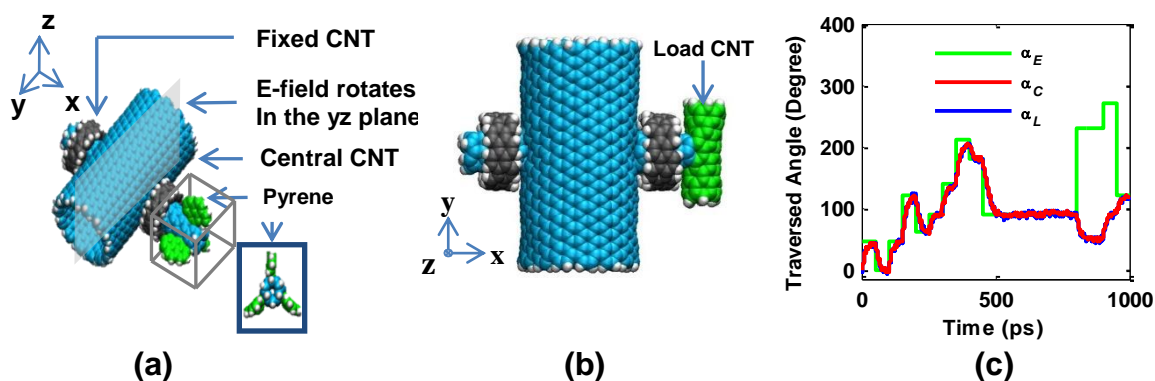
---

[10] http://onlinelibrary.wiley.com/wol1/doi/10.1002/smll.201603978/suppinfo

Figure 3.8. (a) Proposed nanomotor configuration with molecular-scale blades attached as a load. (b) Nanomotor configuration with CNT as a dummy load. (c) Precise position tracking capability of the nanomotor: Traversed angle of the Central (α_C) and the Load CNTs (α_L) with respect to time in response to the abrupt changes in applied electric field angle (α_E).

Now, we present a simulation study to demonstrate how precisely the central CNT along with its load can follow the applied field. For this purpose, we have attached a (6,0) CNT (1.57 nm length) at the end of the wing CNT as a dummy load [Figure 3.8(b)]. We have changed the electric field (1.0 V/nm) angle (α_E) abruptly and observed the corresponding angular displacements at the central CNT (α_C) and the load CNT (α_L). Figure 3.8(c) shows the outcome in an angle vs. time plot (see supplementary movie 7 of Ref 46[11]). It is important to note that, when the electric field changes abruptly, the motor not only tends to align with the applied field, but also tries to minimize its total angular movement. For instance, if the electric field is applied in such a way as $(\alpha_E - \alpha_C) > 90°$, the motor rotates in the opposite direction as discussed previously and travels $180° - (\alpha_E - \alpha_C)$ instead. Therefore, the applied field and the CNTs are separated by an angle of $180°$ from 800 to 950 ps in Figure 3.8(c). Smaller load CNTs follow the central CNT without any lag [$(\alpha_C - \alpha_L) \approx 0$] whereas, larger ones increase the total inertia of the system and bring about a phase lag

---

between the central and load CNTs. The preciseness and control over load rotation highlights the potentiality of using the proposed nanomotor scheme as a nano-robotic arm (similar to a stepper motor) [81].
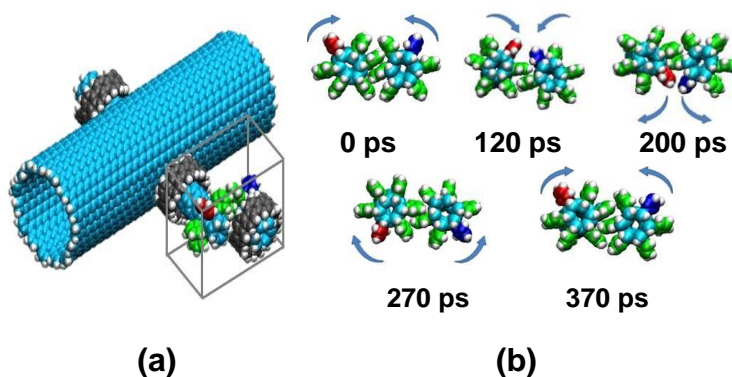
Figure 3.9. (a) Mechanical coupling between the load and the nanomotor with benzene gears. (b) Simulation snapshots of the rotation of gear based load at t=0, 120, 200, 270 and 370 ps respectively.

Figure 3.9 shows the capability of rotating gear-based nanoentities by the proposed nanomotor. In this study, we have attached six benzene molecules to the wing CNTs which work as the gear teeth. This configuration has been mechanically coupled with another CNT (which works as a load) via six benzene teeth around it. Another fixed CNT of the same dimension as the two fixed CNTs of the nanomotor (atoms colored in gray) was used to ensure proper mechanical coupling between the motor and the load. The load is a (6,0) CNT with a length of 1.06 nm. One benzene tooth from each of the sides has been colored differently (red and blue) to show a complete rotation event (see supplementary movie 8 of Ref. 46^{12}). Then, we analyzed whether it is possible to rotate the load CNT by using the gear coupling. For the central CNT length of 3.84 nm, the nanomotor has been found to be incapable of rotating the load properly. However, the motor can exert enough force to rotate the load CNT at 0.125×10^{12} r.p.m. if the length of the central CNT is increased to 7.04 nm.

Since greater number of water molecules gets engaged in interaction when we increase the central CNT length, longer central CNT enhances the load carrying capability of the nanomotor. This can be confirmed by looking into the power produced by the central CNTs. To estimate the torque exerted upon the CNT, we followed the procedure of Kim *et al*. [31] At 1.25×10^{11} r.p.m., the power produced by the 3.84 nm long CNT is about 8.3×10^{-10} W, whereas the value is about 3.53×10^{-9} W (~ 4.3 times higher) for the 7.01 nm CNT. Figure 3.9(b) illustrates the gear-based load rotation event (see supplementary movie 8 of Ref. 46[12]). The applied magnitude of the rotating electric field was 1.0 V/nm.

---

[12]   http://onlinelibrary.wiley.com/wol1/doi/10.1002/smll.201603978/suppinfo

Chapter 4

Conclusions & Future works

4.1   Conclusions

The contributions made in this thesis are as follows-

1. We have explored the electric field induced water dipole orientations to drive a CNT based nanomotor. From molecular dynamics simulations, we have found that if we place a CNT in DI water and apply a rotating electric field of suitable magnitude and angular speed, the CNT follows the field due to the water dipole orientations.

2. We have designed a nanomotor structure based on this principle. Due to the fast responsiveness of the electric field induced CNT orientation in water, the motor has shown ultrahigh-speed (over 10^{11} r.p.m.) performance. Unlike any other previous electrical energy driven nanomotors, availability of a rotating shaft to connect a load is a unique feature of the proposed nanomotor scheme.

3. We have analyzed the role of water dipole orientations on the rotational characteristics of the proposed nanomotor.

4. It has been also found that the force exerted by the motor is enough to rotate molecular-scale blades attached to it (pyrene molecules have been used as blades). We have also studied the capability of our motor in rotating nano-gear based complex structures and its ability to rotate a load at a precise angle as well. Load rotation with a controlled angle highlights the potentiality of using the proposed

nanomotor scheme as a nano-robotic arm. The findings reported in this research could be of interest for NEMS, bio-NEMS, microfluidics and nanofluidics architectures.

4.2   Future works

An interesting extension would be to analyze the performance of the nanomotor incorporating the polarization of the CNTs. Another obvious study would be to investigate the performance of the proposed nanomotor in different polarizable media. Depending on the dipole moment and the density of the fluid, a higher operable speed may be possible in some fluids. It would also be interesting to observe the performance of the nanomotor using nanowires (such as gold, copper nanowires), instead of a CNT. It might also be interesting to find out if the nanomotor can be operated using a circularly polarized light, since circularly polarized light carries a rotating electric field component.

References

[1]   Madou, M. J., *Fundamentals of microfabrication: the science of miniaturization*. CRC press: 2002.

[2]   Wang, H., Pumera, M., "Fabrication of Micro/Nanoscale Motors," *Chemical Reviews,* vol. 115, pp. 8704-8735, 2015.

[3]   Bocquet, L., Charlaix, E., "Nanofluidics, from bulk to interfaces," *Chemical Society Reviews,* vol. 39, pp. 1073-1095, 2010.

[4]   Madou, M. J., *From MEMS to Bio-MEMS and Bio-NEMS: Manufacturing Techniques and Applications*. CRC Press: 2011; Vol. 3.

[5]   Requicha, A. A., "Nanorobots, NEMS, and nanoassembly," *Proceedings of the IEEE,* vol. 91, pp. 1922-1933, 2003.

[6]   Kim, K., Guo, J., Liang, Z., Zhu, F., Fan, D., "Man-made rotary nanomotors: a review of recent developments," *Nanoscale,* vol. 8, pp. 10471-10490, 2016.

[7]   Castro Neto, A. H., Guinea, F., Peres, N. M. R., Novoselov, K. S., Geim, A. K., "The electronic properties of graphene," *Reviews of Modern Physics,* vol. 81, pp. 109-162, 2009.

[8]   Iijima, S., "Helical microtubules of graphitic carbon," *Nature,* vol. 354, pp. 56-58, 1991.

[9]   Odom, T. W., Huang, J.-L., Kim, P., Lieber, C. M., "Atomic structure and electronic properties of single-walled carbon nanotubes," *Nature,* vol. 391, pp. 62-64, 1998.

[10]   Wilder, J. W. G., Venema, L. C., Rinzler, A. G., Smalley, R. E., Dekker, C., "Electronic structure of atomically resolved carbon nanotubes," *Nature,* vol. 391, pp. 59-62, 1998.

[11]   Kataura, H., Kumazawa, Y., Maniwa, Y., Umezu, I., Suzuki, S., Ohtsuka, Y., Achiba, Y., "Optical properties of single-wall carbon nanotubes," *Synthetic metals,* vol. 103, pp. 2555-2558, 1999.

[12]   Wong, E. W., Sheehan, P. E., Lieber, C. M., "Nanobeam mechanics: elasticity, strength, and toughness of nanorods and nanotubes," *science,* vol. 277, pp. 1971-1975, 1997.

[13]   Javey, A., Guo, J., Wang, Q., Lundstrom, M., Dai, H., "Ballistic carbon nanotube field-effect transistors," *nature,* vol. 424, pp. 654, 2003.

[14]   Martin, C. R., Kohli, P., "The emerging field of nanotube biotechnology," *Nature reviews. Drug discovery,* vol. 2, pp. 29, 2003.

[15]   Bauerdick, S., Linden, A., Stampfer, C., Helbling, T., Hierold, C., "Direct wiring of carbon nanotubes for integration in nanoelectromechanical systems," *Journal of Vacuum Science &*

Technology B: Microelectronics and Nanometer Structures Processing, Measurement, and Phenomena, vol. 24, pp. 3144-3147, 2006.

[16]   Hummer, G., Rasaiah, J. C., Noworyta, J. P., "Water conduction through the hydrophobic channel of a carbon nanotube," *Nature,* vol. 414, pp. 188, 2001.

[17]   Rahman, M. M., Chowdhury, M., Alam, M. In *Dynamics of fullerene self-insertion into carbon nanotubes in water*, Electrical and Computer Engineering (ICECE), 2014 International Conference on, IEEE: 2014; pp 365-368.

[18]   Zhang, Q.-L., Jiang, W.-Z., Liu, J., Miao, R.-D., Sheng, N., "Water transport through carbon nanotubes with the radial breathing mode," *Physical review letters,* vol. 110, pp. 254501, 2013.

[19]   Samoylova, O. N., Calixte, E. I., Shuford, K. L., "Molecular dynamics simulations of ion transport in carbon nanotube channels," *The Journal of Physical Chemistry C,* vol. 119, pp. 1659-1666, 2015.

[20]   Shi Kam, N. W., Jessop, T. C., Wender, P. A., Dai, H., "Nanotube molecular transporters: internalization of carbon nanotube− protein conjugates into mammalian cells," *Journal of the American Chemical Society,* vol. 126, pp. 6850-6851, 2004.

[21]   Geng, J., Kim, K., Zhang, J., Escalada, A., Tunuguntla, R., Comolli, L. R., Allen, F. I., Shnyrova, A. V., Cho, K. R., Munoz, D., "Stochastic transport through carbon nanotubes in lipid bilayers and live cell membranes," *Nature,* vol. 514, pp. 612, 2014.

[22]   Ekinci, K., Roukes, M., "Nanoelectromechanical systems," *Review of scientific instruments,* vol. 76, pp. 061101, 2005.

[23]   Despont, M., Brugger, J., Drechsler, U., Dürig, U., Häberle, W., Lutwyche, M., Rothuizen, H., Stutz, R., Widmer, R., Binnig, G., "VLSI-NEMS chip for parallel AFM data storage," *Sensors and Actuators A: Physical,* vol. 80, pp. 100-107, 2000.

[24]   Bailey, S., Amanatidis, I., Lambert, C., "Carbon nanotube electron windmills: a novel design for nanomotors," *Physical review letters,* vol. 100, pp. 256802, 2008.

[25]   Barreiro, A., Rurali, R., Hernández, E. R., Moser, J., Pichler, T., Forro, L., Bachtold, A., "Subnanometer motion of cargoes driven by thermal gradients along carbon nanotubes," *Science,* vol. 320, pp. 775-778, 2008.

[26]   Cai, K., Li, Y., Qin, Q. H., Yin, H., "Gradientless temperature-driven rotating motor from a double-walled carbon nanotube," *Nanotechnology,* vol. 25, pp. 505701, 2014.

[27]   Fan, D., Zhu, F., Cammarata, R., Chien, C., "Controllable high-speed rotation of nanowires," *Physical review letters,* vol. 94, pp. 247208, 2005.

[28]   Fennimore, A., Yuzvinsky, T., Han, W.-Q., Fuhrer, M., Cumings, J., Zettl, A., "Rotational actuators based on carbon nanotubes," *Nature,* vol. 424, pp. 408-410, 2003.

[29]   Guo, J., Kim, K., Lei, K. W., Fan, D., "Ultra-durable rotary micromotors assembled from nanoentities by electric fields," *Nanoscale,* vol. 7, pp. 11363-11370, 2015.

[30]   Keshoju, K., Xing, H., Sun, L., "Magnetic field driven nanowire rotation in suspension," *Applied Physics Letters,* vol. 91, pp. 123114, 2007.

[31]   Kim, K., Xu, X., Guo, J., Fan, D., "Ultrahigh-speed rotating nanoelectromechanical system devices assembled from nanoscale building blocks," *Nature communications,* vol. 5, pp., 2014.

[32]   Kline, T. R., Paxton, W. F., Mallouk, T. E., Sen, A., "Catalytic nanomotors: remote-controlled autonomous movement of striped metallic nanorods," *Angewandte Chemie International Edition,* vol. 44, pp. 744-746, 2005.

[33]   Koumura, N., Zijlstra, R. W., van Delden, R. A., Harada, N., Feringa, B. L., "Light-driven monodirectional molecular rotor," *Nature,* vol. 401, pp. 152-155, 1999.

[34]   Laocharoensuk, R., Burdick, J., Wang, J., "Carbon-nanotube-induced acceleration of catalytic nanomotors," *ACS nano,* vol. 2, pp. 1069-1075, 2008.

[35]   Lee, T.-C., Alarcón-Correa, M., Miksch, C., Hahn, K., Gibbs, J. G., Fischer, P., "Self-propelling nanomotors in the presence of strong Brownian forces," *Nano letters,* vol. 14, pp. 2407-2412, 2014.

[36]   Li, J., Li, T., Xu, T., Kiristi, M., Liu, W., Wu, Z., Wang, J., "Magneto–Acoustic Hybrid Nanomotor," *Nano letters,* vol. 15, pp. 4814-4821, 2015.

[37]   Liu, M., Zentgraf, T., Liu, Y., Bartal, G., Zhang, X., "Light-driven nanoscale plasmonic motors," *Nature nanotechnology,* vol. 5, pp. 570-573, 2010.

[38]   Ma, X., Jannasch, A., Albrecht, U.-R., Hahn, K., Miguel-López, A., Schäffer, E., Sánchez, S., "Enzyme-Powered Hollow Mesoporous Janus Nanomotors," *Nano letters,* vol. 15, pp. 7043-7050, 2015.

[39]   Mishra, P., Hill, J. P., Vijayaraghavan, S., Rossom, W. V., Yoshizawa, S., Grisolia, M., Echeverria, J., Ono, T., Ariga, K., Nakayama, T., "Current-driven supramolecular motor with in situ surface chiral directionality switching," *Nano letters,* vol. 15, pp. 4793-4798, 2015.

[40]   Santamaria-Holek, I., Reguera, D., Rubi, J., "Carbon-nanotube-based motor driven by a thermal gradient," *The Journal of Physical Chemistry C,* vol. 117, pp. 3109-3113, 2013.

[41]   Somada, H., Hirahara, K., Akita, S., Nakayama, Y., "A molecular linear motor consisting of carbon nanotubes," *Nano letters,* vol. 9, pp. 62-65, 2008.

[42]   Srivastava, S. K., Guix, M., Schmidt, O. G., "Wastewater mediated activation of micromotors for efficient water cleaning," *Nano letters,* vol. 16, pp. 817-821, 2015.

[43]   Sundararajan, S., Lammert, P. E., Zudans, A. W., Crespi, V. H., Sen, A., "Catalytic motors for transport of colloidal cargo," *Nano letters,* vol. 8, pp. 1271-1276, 2008.

[44]   Jianrong, C., Yuqing, M., Nongyue, H., Xiaohua, W., Sijiao, L., "Nanotechnology and biosensors," *Biotechnology advances,* vol. 22, pp. 505-518, 2004.

[45]   Li, C., Thostenson, E. T., Chou, T.-W., "Sensors and actuators based on carbon nanotubes and their composites: a review," *Composites Science and Technology,* vol. 68, pp. 1227-1249, 2008.

[46]   Rahman, M. M., Chowdhury, M. M., Alam, M., "Rotating-Electric-Field-Induced Carbon-Nanotube-Based Nanomotor in Water: A Molecular Dynamics Study," *Small,* vol. 13, pp. 1603978-1 - 1603978-10, 2017.

[47]   Tasis, D., Tagmatarchis, N., Bianco, A., Prato, M., "Chemistry of carbon nanotubes," *Chemical reviews,* vol. 106, pp. 1105-1136, 2006.

[48]   Sanchez, S., Soler, L., Katuri, J., "Chemically Powered Micro-and Nanomotors," *Angewandte Chemie International Edition,* vol. 54, pp. 1414-1444, 2015.

[49]   Wilson, M. R., Solà, J., Carlone, A., Goldup, S. M., Lebrasseur, N., Leigh, D. A., "An autonomous chemically fuelled small-molecule motor," *Nature,* vol. 534, pp. 235-240, 2016.

[50]   Bishop, J. D., Klavins, E., "An improved autonomous DNA nanomotor," *Nano letters,* vol. 7, pp. 2574-2577, 2007.

[51]   He, Y., Wu, J., Zhao, Y., "Designing catalytic nanomotors by dynamic shadowing growth," *Nano letters,* vol. 7, pp. 1369-1375, 2007.

[52]   Xu, Z., Wang, C., Sheng, N., Hu, G., Zhou, Z., Fang, H., "Manipulation of a neutral and nonpolar nanoparticle in water using a nonuniform electric field," *The Journal of chemical physics,* vol. 144, pp. 014302, 2016.

[53]   Wang, B., Král, P., "Chemically tunable nanoscale propellers of liquids," *Physical review letters,* vol. 98, pp. 266102, 2007.

[54]   Humphrey, W., Dalke, A., Schulten, K., "VMD: visual molecular dynamics," *Journal of molecular graphics,* vol. 14, pp. 33-38, 1996.

[55]   DeLano, W. L., PyMOL. In *Secondary "PyMOL"*, 2002.

[56]   Hess, B., Kutzner, C., Van Der Spoel, D., Lindahl, E., "GROMACS 4: algorithms for highly efficient, load-balanced, and scalable molecular simulation," *Journal of chemical theory and computation,* vol. 4, pp. 435-447, 2008.

[57]   Jorgensen, W. L., Maxwell, D. S., Tirado-Rives, J., "Development and testing of the OPLS all-atom force field on conformational energetics and properties of organic liquids," *Journal of the American Chemical Society,* vol. 118, pp. 11225-11236, 1996.

[58]   Zou, J., Ji, B., Feng, X.-Q., Gao, H., "Self-assembly of single-walled carbon nanotubes into multiwalled carbon nanotubes in water: molecular dynamics simulations," *Nano letters,* vol. 6, pp. 430-434, 2006.

[59]   Rahman, M. M., Chowdhury, M., Rosul, M., Alam, M., "Effect of bending on the molecular transport along carbon nanotubes," *physica status solidi (b),* vol. 254, pp., 2017.

[60]   Tu, Q., Yang, Q., Wang, H., Li, S., "Rotating carbon nanotube membrane filter for water desalination," *Scientific Reports,* vol. 6, pp. 26183, 2016.

[61]   LeSar, R., *Introduction to computational materials science: fundamentals to applications*. Cambridge University Press: 2013.

[62]   Jorgensen, W. L., Chandrasekhar, J., Madura, J. D., Impey, R. W., Klein, M. L., "Comparison of simple potential functions for simulating liquid water," *The Journal of chemical physics,* vol. 79, pp. 926-935, 1983.

[63]   Abadir, G. B., Walus, K., Pulfrey, D. L., "Bias-dependent amino-acid-induced conductance changes in short semi-metallic carbon nanotubes," *Nanotechnology,* vol. 21, pp. 015202, 2010.

[64]   Winarto, Takaiwa, D., Yamamoto, E., Yasuoka, K., "Separation of water-ethanol solutions with carbon nanotubes and electric fields," *Physical Chemistry Chemical Physics,* vol. 18, pp. 33310-33319, 2016.

[65]   Hao, X., Qiang, H., Xiaohu, Y., "Buckling of defective single-walled and double-walled carbon nanotubes under axial compression by molecular dynamics simulation," *Composites Science and Technology,* vol. 68, pp. 1809-1814, 2008.

[66]   Guo, X., Su, J., Guo, H., "Electric field induced orientation and self-assembly of carbon nanotubes in water," *Soft Matter,* vol. 8, pp. 1010-1016, 2012.

[67]   Settanni, G., Fersht, A. R., "High Temperature Unfolding Simulations of the TRPZ1 Peptide," *Biophysical Journal,* vol. 94, pp. 4444-4453, 2008.

[68]   Kelich, P., Asadinezhad, A., "Molecular Dynamics Insights into Behavior of Poly(ethylene succinate) Single Chain on Carbon Nanotube Surface," *The Journal of Physical Chemistry C,* vol. 119, pp. 26143-26153, 2015.

[69]   Mochizuki, K., Pattenaude, S. R., Ben-Amotz, D., "Influence of Cononsolvency on the Aggregation of Tertiary Butyl Alcohol in Methanol–Water Mixtures," *Journal of the American Chemical Society,* vol. 138, pp. 9045-9048, 2016.

[70]   Daub, C. D., Bratko, D., Ali, T., Luzar, A., "Microscopic dynamics of the orientation of a hydrated nanoparticle in an electric field," *Physical review letters,* vol. 103, pp. 207801, 2009.

[71]   Nosé, S., "A molecular dynamics method for simulations in the canonical ensemble," *Molecular physics,* vol. 52, pp. 255-268, 1984.

[72]   Berendsen, H. J., Postma, J. v., van Gunsteren, W. F., DiNola, A., Haak, J., "Molecular dynamics with coupling to an external bath," *The Journal of chemical physics,* vol. 81, pp. 3684-3690, 1984.

[73]   Darden, T., York, D., Pedersen, L., "Particle mesh Ewald: An N· log (N) method for Ewald sums in large systems," *The Journal of chemical physics,* vol. 98, pp. 10089-10092, 1993.

[74]   Zasetsky, A. Y., "Dielectric relaxation in liquid water: two fractions or two dynamics?," *Physical review letters,* vol. 107, pp. 117601, 2011.

[75]   Liu, C., Lv, Y., Li, Z., "Fluid transport in nanochannels induced by temperature gradients," *The Journal of chemical physics,* vol. 136, pp. 114506, 2012.

[76]   Bresme, F., Lervik, A., Bedeaux, D., Kjelstrup, S., "Water polarization under thermal gradients," *Physical review letters,* vol. 101, pp. 020602, 2008.

[77]   Rinne, K. F., Gekle, S., Bonthuis, D. J., Netz, R. R., "Nanoscale pumping of water by AC electric fields," *Nano letters,* vol. 12, pp. 1780-1783, 2012.

[78]   Xu, X., Li, H., Hasan, D., Ruoff, R. S., Wang, A. X., Fan, D., "Near-field enhanced plasmonic-magnetic bifunctional nanotubes for single cell bioanalysis," *Advanced Functional Materials,* vol. 23, pp. 4332-4338, 2013.

[79]   Peiris, P. M., Bauer, L., Toy, R., Tran, E., Pansky, J., Doolittle, E., Schmidt, E., Hayden, E., Mayer, A., Keri, R. A., "Enhanced delivery of chemotherapy to tumors using a multicomponent nanochain with radio-frequency-tunable drug release," *ACS nano,* vol. 6, pp. 4157-4168, 2012.

[80]   Gao, W., Wang, J., "Synthetic micro/nanomotors in drug delivery," *Nanoscale,* vol. 6, pp. 10486-10494, 2014.

[81]   Ding, B., Seeman, N. C., "Operation of a DNA robot arm inserted into a 2D DNA crystalline substrate," *Science,* vol. 314, pp. 1583-1585, 2006.